SANS and Cryo-TEM Study of Self-Assembled Diblock Copolypeptide Hydrogels with Rich Nano- through Microscale Morphology

Darrin J. Pochan,* Lisa Pakstis, and Bulent Ozbas

Materials Science and Engineering and Delaware Biotechnology Institute, University of Delaware, Newark, Delaware 19716

Andrew P. Nowak and Timothy J. Deming

Departments of Materials and Chemistry, University of California at Santa Barbara, Santa Barbara, California 93106

Hydrogels for superabsorption, drug delivery matrices, and tissue engineering scaffolds have been traditionally constructed with high molecular weight, hydrophilic polymers that are physically cross-linked through entanglements or chemically cross-linked into a network.[1,2] Constituent polymers can include synthetic polyalcohols and ethers like PVA[3] and PEG/PEO,[4−6] biopolymers such as collagen and polysaccharides[7−11] and biopolymer−PEG hybrids,[12] polyacids[13] and polyacid−PEG hybrids,[14] or biomimetic polymers and globular proteins.[15,16] Each of these classes of gelator polymers can be chosen for a particular set of network properties required in the end use of the material (biodegradability in the case of drug delivery network, biocompatibility and nontoxicity in tissue engineering scaffolding). At the same time, all gels formed from the entanglement/cross-linking of high molecular weight linear polymers exhibit similar morphological properties. There is no controllable ordering or discernible nano- and microstructure of the innate gel matrix material beyond the local intermolecular associations on the molecular level, unless added via processing such as freeze−thaw cycling[17] or particulate leeching and foaming in the case of tissue scaffolds.[18,19]

Recently, construction of hydrogels via self-assembling, supramolecular mechanisms of relatively small molecules has been explored to produce gel networks with tunable, responsive properties.[20−24] We have initiated work into the self-assembly behavior of block copolypeptides[25,26] with which one can molecularly engineer rheological and morphological properties in the final assembled materials through molecular parameters such as architecture (diblock vs triblock) and block secondary structure (α-helix vs β-sheet forming amino acid sequences). We have recently observed the aqueous self-assembly gelation behavior of a set of amphiphilic diblock polypeptides into hydrogels with rich nano- and microscale morphology.[26] The morphology is hierarchical in nature, consisting of an interpenetrating membrane network on the nanoscale and a bicontinuous, heterogeneous morphology containing the gel matrix and pure water channels on the microscale. Presented here is the first small-angle neutron scattering (SANS) exploration of the gel matrix nanoscale morphology combined with cryogenic transmission electron microscopy (cryoTEM) and laser scanning confocal microscopy (LSCM). We observed a diffraction-like SANS response in the 50−100 nm length scale indicative of a regular ordering within the self-assembled gel matrix scaffolding.

The polymer studied, denoted $K_{180}(LV)_{20}$, is an amphiphilic diblock polypeptide of average total length of 200 amino acid residues with a 90 mol % hydrophilic block consisting of homopoly-L-lysine and 10 mol % hydrophobic block consisting of a statistical mixture of 70 mol % L-leucine and 30 mol % L-valine (total molecular weight polydispersity was ∼1.2 as determined by size exclusion chromatography).[27] The gelation behavior was studied in a dilute concentration regime from 0.5 to 5.0 wt %. Hydrogel samples for SANS measurements and cryo-TEM nanoscale morphology observation were prepared by dissolution of copolymer in D_2O. SANS experiments were performed on beamline NG3[28] at the National Center for Neutron Research, National Institute of Standards and Technology. Cryo-TEM imaging was performed on the gels by directly pressing carbon-coated TEM support grids into the gel and consequently removing a thin film of gel matrix; the majority of the captured films has a thickness ∼100 nm, allowing observation in the microscope. The grids were then plunged into liquid ethane for gel vitrification directly on-grid and transferred to the TEM for unstained, in situ observation at 200 kV. Samples for microscale morphology characterization via LSCM were prepared by dissolution in H_2O already containing a trace amount of hydrophobic fluorescent dye. This allowed the incorporation of the dye into the gel matrix during self-assembly and inhibited artifacts that occur due to the limited diffusion of the dye if added to an already formed gel.

Figure 1 contains SANS profiles of a $K_{180}(LV)_{20}$ concentration series with the prominent characteristic of a scattering maximum at low q that shifts to consistently lower q with lowering concentration. The presence of the scattering maxima reveals a regular structure within the gel matrix presumably formed during the self-assembly process with $d \sim 2\pi q_{max}$ spanning 46 nm in the 5.0 wt % block copolypeptide sample up to 76 nm in the 0.5 wt % sample. The scattering maxima lose intensity as the concentration of polypeptide drops, with the peak essentially disappearing at 0.5 wt % polypeptide. The gel structure underlying this diffraction-like scattering was stable up to at least 75 °C as revealed in both the persistence of the peak in SANS measurements at high temperatures for the 5.0 and 2.0 wt % hydrogels (Figure 2) and visual inspection of benchtop-heated samples. A nonlinear least-squares fit of the data shows that q_{max} varies with ϕ^α, where ϕ is the volume percent of polymer in the gel, with $\alpha = 0.22$ indicative of some type of interparticle expansion with dilution of the gel scaffolding. Similar peaks and scaling exponents with concentration have been observed in homopolymer polyelectrolyte and dendrimer solution SANS experiments, presumably due to a regular intercluster packing or intermolecular spacing, respectively.[29,30] Solution ordering has also been observed in synthetic block copolymer gels, although in these cases discrete micelles order onto a cubic lattice.[31,32] However, these literature examples of solution structure all occurred at much smaller spacings (where $d_{dendrimer} < 25$ nm, $d_{polyelectrolyte} < 20$ nm, and $d_{block\ copolymer} \sim 24$ nm) and, in the case of block copolymer solutions, much higher concentrations (polymer = 40 wt %) than observed in these diblock copolypeptide self-assembled gels. We are unaware of any previous observations of
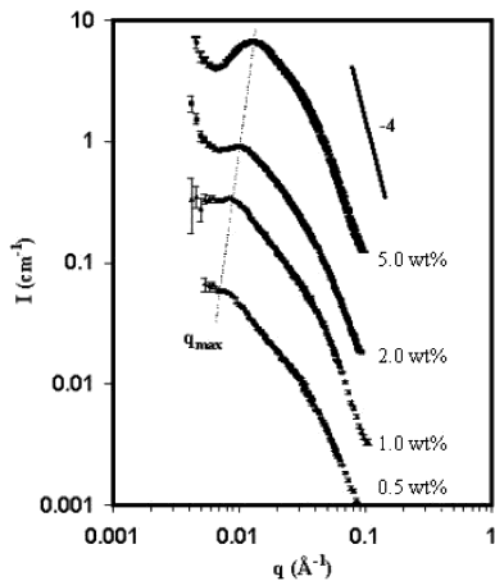
Figure 1. Small-angle neutron scattering from 5.0, 2.0, 1.0, and 0.5 wt % $K_{180}(LV)_{20}$ diblock copolypeptide gels in D_2O where $q = (4\pi/\lambda) \sin \theta/2$, is the neutron wavelength, and θ is the scattering angle. Scattering curves are vertically offset from the 5.0 wt % curve for clarity. The −4 Porod scaling for scattering from an infinitely sharp interface is schematically shown at high q. The approximately −4 scaling in the 5 wt % scattering curve indicates a well-defined, smooth, sharp interface between the self-assembled diblock copolypeptide structures and the D_2O solvent.[34] In the more dilute gels the high q slope is slightly less than −4, implying less well-defined interfaces between the scaffold and the D_2O matrix.
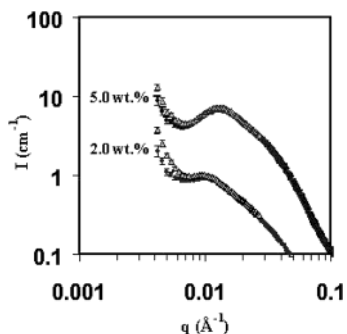
Figure 2. Small-angle neutron scattering from 5.0 and 2.0 wt % $K_{180}(LV)_{20}$ gels at room temperature (closed symbols) and 75 °C (open symbols). Stability of underlying gel scaffold structure at high temperatures is evident through unchanged q_{max} and intensity or scattering maxima.

apparent regular ordering in such a dilute, self-assembled system that produces a rigid gel material.

Figure 3A,B contains real-space microscopy data on the 5.0 wt % $K_{180}(LV)_{20}$ hydrogels revealing both the microstructure, via LSCM, and nanostructure, via cryo-TEM, of the self-assembled peptide gel system. On the microscale the gel was heterogeneous with large 1−30 μm water-rich or pure water pores (black regions with no hydrophobic fluorescent dye) surrounded by gel matrix regions (bright regions due to incorporation of hydrophobic dye during self-assembly). This microscale porous structure was observed at all concentrations of $K_{180}(LV)_{20}$ studied. Cryo-TEM in Figure 3B of the gel matrix regions provided a direct, in situ observation of the self-assembled block copolypeptide gel matrix structure. The gel scaffold apparently consisted of interpenetrating membranous structures that remained stable laterally for at most several hundred nanometers before
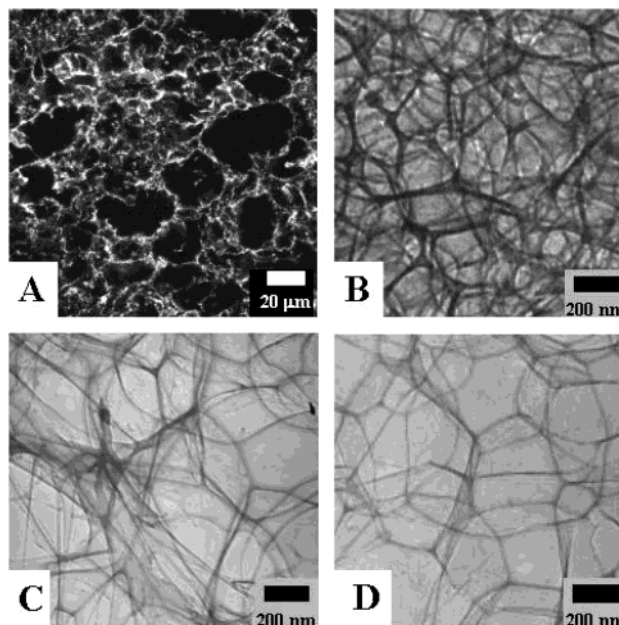
Figure 3. (A) Laser scanning confocal micrograph of 5.0 wt % $K_{180}(LV)_{20}$ in H_2O containing porous, heterogeneous microstructure. (B−D) Cryogenic transmission electron microscopy results of 5.0, 2.0, and 1.0 wt % $K_{180}(LV)_{20}$ in D_2O showing interconnected membrane, cellular nanostructure of gel matrix (dark) surrounded/filled by vitreous water (light).

forming holes and/or forming struts to out-of-plane membranes. Cryo-TEM of 2.0 and 1.0 wt % gels, with similar but more dilute morphology, is shown in Figure 3C,D. This interconnected membrane structure produced a cellular scaffold and is representative of what was observed in all of the $K_{180}(LV)_{20}$ gels studied via SANS. Within the cellular scaffold, particularly in the 1.0 and 2.0 wt % gels, the lateral distances observed between neighboring cell membrane walls is >100 nm (at least locally in the regions represented in the micrographs) while the largest spacing observed via SANS is ~80 nm in the 0.5 wt % gel. We propose the SANS maxima observed in the current q range are actually higher order harmonics of the long spacing, q^*, arising from the first-order interparticle scattering between neighboring block copolypeptide self-assembled membranes constituting the cellular network. The swelling of the space between neighboring solution structures on dilution, as measured by SANS, is consistent with the concentration dependence of interparticle correlations in solution. Assuming the peak observed at $q_{max} = 0.14$ Å^{-1} in the 5 wt % gel is actually the third-order harmonic $3q^*$, q^* would occur at $q^* = 0.0046$, corresponding to an average long spacing of approximately 140 nm. In the 1 wt % hydrogel $3q^*$ at the observed 0.009 Å^{-1} would have a first-order peak at $q^* = 0.003$ Å^{-1} and give a long spacing of ~210 nm. To our knowledge, a regular gel structure on the hundreds of nanometers length scale is unprecedented.

The innate 3-dimensional nano- and microstructure of the hydrogels formed during molecular self-assembly, combined with their peptide backbone, makes these hierarchically structured gels intriguing candidates for advanced biomaterials applications. Specifically, the inherent hydrogel microporosity is well suited to support in vitro cell motility and proliferation, in addition to allow cell growth medium solution transport, all critical ingredients for successful tissue engineering.[18,19] The peptidic nature of the gel membrane scaffold allows the

engineering of noncytotoxic matrices through the correct choice of hydrophilic amino acid blocks,[33] in addition to the potential doping in of blocks functionalized with specific cell binding site sequences and appropriate growth factors for desired cell growth and differentiation. Future work will explore these tissue engineering possibilities.

References and Notes

(1) Peppas, N. A.; Huang, Y.; Torres-Lugo, M.; Ward, J. H.; Zhang, J. *Annu. Rev. Biomed. Eng.* **2000**, *2*, 9−29.
(2) Langer, R. *Acc. Chem. Res.* **2000**, *33*, 94−101.
(3) Hassan, C. M.; Peppas, N. A. *Macromolecules* **2000**, *33*, 2472−2479.
(4) Riley, S. L.; Dutt, S.; de la Torre, R.; Chen, A. C.; Sah, R. L.; Ratcliffe, A. *J. Mater. Sci.: Mater. Med.* **2001**, *12*, 983−990.
(5) Mann, B. K.; Gobin, A. S.; Tsai, A. T.; Schmedlen, R. H.; West, J. L. *Biomaterials* **2001**, *22*, 3045−3051.
(6) Zheng, Y. J.; Andreopoulos, F. M.; Micic, M.; Huo, Q.; Pham, S. M.; Leblanc, R. M. *Adv. Funct. Mater.* **2001**, *11*, 37−40.
(7) Ross-Murphy, S. B. *Imaging Sci. J.* **1997**, *45*, 205−209.
(8) Ross-Murphy, S. B.; Wang, Q.; Ellis, P. R. *Macromol. Symp.* **1998**, *127*, 13−21.
(9) Ramakrishnan, S.; Prud'homme, R. K. *J. Rheol.* **2000**, *44*, 885−896.
(10) Nomura, Y.; Toki, S.; Ishii, Y.; Shirai, K. *Biomacromolecules* **2001**, *2*, 105−110.
(11) Chellat, F.; Tabrizian, M.; Dumitriu, S.; Chornet, E.; Magny, P.; Rivard, C. H.; Yahia, L. *J. Biomed. Mater. Res.* **2000**, *51*, 107−116.
(12) Demers, N.; Agostinelli, E.; Averill-Bates, D. A.; Fortier, G. *Biotechnol. Appl. Biochem.* **2001**, *33*, 201−207.
(13) GrosseSommer, A.; Prudhomme, R. K. *J. Controlled Release* **1996**, *40*, 261−267.
(14) Metters, A. T.; Anseth, K. S.; Bowman, C. N. *J. Phys. Chem. B* **2001**, *105*, 8069−8076.
(15) Park, Y. J.; Liang, J. F.; Yang, Z. Q.; Yang, V. C. *J. Controlled Release* **2001**, *75*, 37−44.
(16) Kavanagh, G. M.; Clark, A. H.; Gosal, W. S.; Ross-Murphy, S. B. *Macromolecules* **2000**, *33*, 7029−7037.
(17) Hassan, C. M.; Peppas, N. A. *J. Appl. Polym. Sci.* **2000**, *76*, 2075−2079.
(18) Martin, I.; Shastri, V. P.; Padera, R. F.; Yang, J.; Mackay, A. J.; Langer, R.; Vunjak-Novakovic, G.; Freed, L. E. *J. Biomed. Mater. Res.* **2001**, *55*, 229−235.
(19) Mooney, D. J.; Park, S.; Kaufmann, P. M.; Sano, K.; McNamara, K.; Vacanti, J. P.; Langer, R. *J. Biomed. Mater. Res.* **1995**, *29*, 959−965.
(20) Caplan, M. R.; Schwartzfarb, E. M.; Zhang, S. G.; Kamm, R. D.; Lauffenburger, D. A. *Biomaterials* **2002**, *23*, 219−227.
(21) Jung, J. H.; John, G.; Masuda, M.; Yoshida, K.; Shinkai, S.; Shimizu, T. *Langmuir* **2001**, *17*, 7229−7232.
(22) Hartgerink, J. D.; Beniash, E.; Stupp, S. I. *Science* **2001**, *294*, 1684−1688.
(23) Tae, G.; Kornfield, J. A.; Hubbell, J. A.; Johannsmann, D.; Hogen-Esch, T. E. *Macromolecules* **2001**, *34*, 6409−6419.
(24) Collier, J. H.; Hu, B. H.; Ruberti, J. W.; Zhang, J.; Shum, P.; Thompson, D. H.; Messersmith, P. B. *J. Am. Chem. Soc.* **2001**, *123*, 9463−9464.
(25) Yu, M.; Nowak, A. P.; Deming, T. J.; Pochan, D. J. *J. Am. Chem. Soc.* **1999**, *121*, 12210−12211.
(26) Nowak, A. P.; Breedveld, V.; Pine, D. J.; Pakstis, L.; Ozbas, B.; Pochan, D. J.; Deming, T. J. *Nature (London)*, **2002**, *417*, 424−428.
(27) Deming, T. J. *Macromolecules* **1999**, *32*, 4500−4502.
(28) SANS instrument description: The neutron beam was monochromated to 9 Å with a velocity selector having a wavelength spread of 0.15 ($\Delta\lambda/\lambda = 0.15$). The scattered neutrons were detected by a 64 cm × 64 cm two-dimensional detector using three different sample-to-detector distances, 13, 4, and 1.5 m. These configurations allow values of the scattering wavevector q in the range $0.004 < q$ (Å^{-1}) < 0.500. Here q is the scattering vector defined as $q = (4/\lambda) \sin(\theta/2)$, where λ is the neutron wavelength (9 Å) and θ the scattering angle. The resulting data were corrected for background electronic noise, detector inhomogeneity, empty cell scattering, and solvent scattering. The uncertainties of the $I(q)$ vs q individual data points are calculated statistically from the number of averaged detector counts.
(29) Ermi, B. D.; Amis, E. J. *Macromolecules* **1998**, *31*, 7378−7384.
(30) Nisato, G.; Ivkov, R.; Amis, E. J. *Macromolecules* **1999**, *32*, 5895−5900.
(31) Hamley, I. W.; Mortensen, K.; Yu, G. E.; Booth, C. *Macromolecules* **1998**, *31*, 6958−6963.
(32) Prudhomme, R. K.; Wu, G. W.; Schneider, D. K. *Langmuir* **1996**, *12*, 4651−4659.
(33) Pakstis, L.; Nowak, Ozbas, B.; A. P.; Deming, T. J.; Pochan, D. J. In preparation.
(34) Porod, G. In *Small-Angle X-ray Scattering*; Glatter, O., Kratky, O., Eds.; Academic Press: London, 1982; p 17.